Received: 16 January 2023 | Revised: 14 April 2023 | Accepted: 29 April 2023

DOI: 10.1111/jace.19204

Journal of the American Ceramic Society

RESEARCH ARTICLE

Direct comparison of surface crystal growth kinetics in chalcogenide glass measured by microscopy and DSC

Jana Shánělová[1] | **Pavla Honcová**[2] | **Jiří Málek**[1] | **Antonio Perejón**[3,4] | **Luis A. Pérez-Maqueda**[3]

[1]Department of Physical Chemistry, Faculty of Chemical Technology, University of Pardubice, Pardubice, Czech Republic

[2]Department of Inorganic Technology, Faculty of Chemical Technology, University of Pardubice, Pardubice, Czech Republic

[3]Instituto de Ciencia de Materiales de Sevilla (C.S.I.C.—Univ. Sevilla), Sevilla, Spain

[4]Departamento de Química Inorgánica, Facultad de Química, Universidad de Sevilla, Sevilla, Spain

Correspondence
Jana Shánělová, Department of Physical Chemistry, Faculty of Chemical Technology, University of Pardubice, 53210 Pardubice, Czech Republic.
Email: Jana.Shanelova@upce.cz

Funding information
EU Next Generation funds; Ministry of Science and Innovation, Spain (MICINN) Spanish Government; University of Pardubice

Abstract

Surface crystallization in fine powder $Se_{70}Te_{30}$ chalcogenide glass was studied by differential scanning calorimetry (DSC) and optical microscopy. A complex kinetic analysis of these experimental data reveals that the contracting sphere mechanism (R3 model) is the rate determining step of crystal growth, and the conventional Johnson–Mehl–Avrami–Kolmogorov model cannot be used in this case. Moreover, it is clearly shown that the particle size distribution should be considered in crystallization studies. Actually, when the particle size effect is taken into account, the simulated DSC curves for the R3 model agree very well with the experimental data over the entire temperature range. The crystallization kinetics determined from the nonisothermal DSC data are consistent with previously reported isothermal crystallization data for the same powder fraction. The crystal growth rate calculated from isothermal and nonisothermal DSC data agrees very well with the microscopically measured surface and bulk crystal growth rate.

KEYWORDS
chalcogenide glass, contracting sphere model, crystal growth, DSC, kinetics

1 | INTRODUCTION

Phase transformations such as the crystallization of glasses are of great interest in ceramics science. Currently, differential thermal analysis (DTA) and differential scanning calorimetry (DSC) are the most widely used experimental techniques to study crystallization kinetics in glasses, amorphous materials, and supercooled liquids. Crystallization is typically considered in two separate stages: nucleation and crystal growth. However, nucleation is difficult to study experimentally, unlike subsequent crystal growth. Several models have been proposed for the kinetic description of the crystallization process, which should provide information on the mechanism of nucleation and growth. The effort is to find possible correlations between the molecular structure and the nucleation and growth mechanism and to identify processes that control crystallization.[1–4]

Johnson–Mehl–Avrami–Kolmogorov (JMAK) theory is one of the most frequently used approaches to describe crystallization in the volume of bulk materials,[5–9] and a simple method to test the applicability of the JMAK model for describing isothermal and nonisothermal DTA and DSC data has been proposed.[10] Nevertheless, it seems that crystallization at glass surfaces (grains, powders, etc.) represents a more complex transformation where the JMAK theory might fail to describe the experimental data.[11] Müller[12] proposed a kinetic model of surface-induced glass crystallization that considers the grain size of glass powder, a constant density of surface nuclei, and a steadily increasing temperature throughout the crystallization. Weinberg[13] proposed an alternative model for the surface and bulk crystallization of spherical particles. Reis and Zanotto[14] recently developed a simple model that describes the kinetics of particle phase transformation starting from the surface and internal nucleation sites. This model was successfully tested using DSC crystallization data for diopside spherical powders with a finite number of surface sites and lithium disilicate glass particles that exhibit simultaneous surface and internal growth.[14] Ferreira et al.[15] proposed another model to describe the heterogeneous crystallization kinetics of spherical particles. Some authors observed a change in crystallization kinetics with powder size.[16–19] Fernandes et al.[20,21] studied the effect of irregular particle shapes. Several methods were also developed to estimate the crystal growth rate for silicate glasses from DTA or DSC data.[22–25]

Despite recent efforts to describe the crystallization kinetics of silicate glasses, few studies have been dedicated to other types of glassy materials. One of the first attempts to crystallize chalcogenide glasses in this sense was by Henderson and Ast,[26] who combined isothermal DSC measurements of powder samples, viscosity in a supercooled liquid, and in situ microscopic measurement of crystal growth. The effect of the sample form (fine powder, coarse powder, and bulk) was studied for Ge–Sb–S glass.[27] Significant crystallization studies were reported for phase change materials of chalcogenides.[28,29] Some authors also focused their attention on the combined study of the kinetics of crystal growth of chalcogenide glasses by microscopy and DSC.[30–33] The crystal growth rate in thin chalcogenide films was calculated using a correlation between DSC data (described by the JMAK model) and microscopy data.[29,34,35] However, to our knowledge, there are not as many articles that provide a model for the direct calculation of crystal growth data from DSC measurements.[36]

This paper quantitatively compares the surface crystal growth kinetics in a chalcogenide glass measured by microscopy and DSC. Both methods monitor the process studied differently. Isothermal crystal growth rates in bulk samples are measured directly by optical and infrared microscopy, while DSC provides a direct information about the heat flow released during the crystallization process in fine powder under nonisothermal conditions. The crystal growth rate is calculated by precise kinetic analysis and fitting of the DSC data using the contracting sphere model involving the grain size distribution. These results are very close to the microscopically observed growth rates. This novel complex kinetic analysis reveals that the contracting sphere mechanism is the rate determining step of crystal growth in the fine powder of $Se_{70}Te_{30}$ chalcogenide glass.

2 | METHODOLOGY

2.1 | Experimental procedure

We used $Se_{70}Te_{30}$ chalcogenide glass as a model system. It was prepared from pure elements (5 N, Sigma–Aldrich) by using the melt quenching technique. The elements were weighed into a silica ampoule, evacuated, and then sealed. The ampoule was heated in a rocking furnace at 923 K for 24 h. The glass was prepared from its melt by quenching the ampoule in water. The total mass of the prepared glass ingot was approximately 10 g. The amorphous nature of the glass was verified by X-ray diffraction (XRD) and optical microscopy.

Crystallization of the glass was studied using a Q200 differential scanning calorimeter (TA Instruments). The calorimeter was calibrated by melting pure metals (In, Zn). Dry nitrogen was used as purge gas (20 cm^3 min^{-1}). The glass was ground and separated using sieves into fractions with a particle size of 20–50 μm. The prepared powder was stored in a closed bottle at room temperature for several days prior to DSC analysis. The sample mass of approximately 8 mg of powder was weighed into an aluminium pan and sealed for DSC measurement, with the empty pan serving as a reference. The samples were measured by using a specific temperature program reflecting the relaxation phenomena described in Ref.[37] First, the samples were briefly annealed at a temperature just above T_g (5 min at 343 K) to erase any previous thermal history. In the second step, the samples were cooled to 293 K at a rate of 10 K min^{-1}. Immediately following, the samples were heated to 453 K at a heating rate of 2, 5, or 10 K min^{-1}. OriTas software[38] was used to analyze the kinetics of the experimental DSC data.

Surface crystal growth was monitored using an Olympus BX51 optical microscope equipped with a standard DP72 camera and an infrared XM10 camera operating in reflection mode. The bulk glass samples were annealed in a computer-controlled furnace at selected temperatures in the 352–407 K range for different periods of time

(the temperature was held constant to within ±0.5 K). The samples were then quenched to room temperature. Crystals were formed during annealing in the form of spherical (hemispherical) aggregates in the bulk volume (on the surface). Similar crystal shapes were described by Barták et al.[39] The samples were broken to determine the thickness of the crystalline surface layer and also to detect crystals within the sample volume. For a given temperature and time, a sample was analyzed in different places, with 20–40 values accumulated. Volume crystallization is entirely consistent with previously reported data.[39]

2.2 | Analysis of DSC data

The output of DSC during crystallization is the heat flow Φ as a function of time t or temperature T, and is expressed as[40]

$$\Phi = \Delta H \cdot \frac{d\alpha}{dt} \tag{1}$$

where ΔH is the enthalpy change of the process and α is a conversion. The reaction rate $d\alpha/dt$ is given by

$$\frac{d\alpha}{dt} = k(T) \cdot f(\alpha) \tag{2}$$

The first part $k(T)$ of this equation is a rate constant that depends on the temperature T, and is usually described by the Arrhenius equation:

$$k(T) = A \cdot e^{-\frac{E}{RT}} \tag{3}$$

where A is the preexponential factor, E is the activation energy, and R is the molar gas constant.

The second part $f(\alpha)$ of the reaction rate equation represents a kinetic model. The selection of an appropriate kinetic model to describe the experimental data is very important for the correct interpretation of the mechanism and to understand the correlation between the parameters of the model and the mechanism of the process.

Several methods are available to select the model. One method involves analyzing the symmetry of the DSC peak.[41] The shape index S expresses an inflection asymmetry that can be determined by using tangents at the inflection points at T_1 and T_2 of the nonisothermal DSC curve. The dependence of the calculated shape index on the ratio T_2/T_1 helps determine the most suitable kinetic model.[41] Another method to select the kinetic model is based on the symmetry of the DSC peak and uses data transformed into normalized functions $y(\alpha)$ and $z(\alpha)$.[40,42]

For nonisothermal DSC data, the functions $y(\alpha)$ and $z(\alpha)$ are given by

$$y(\alpha) = \Phi \cdot e^{\frac{E}{RT}} \tag{4}$$

$$z(\alpha) = \Phi \cdot T^2 \tag{5}$$

The combined kinetic analysis described by Pérez-Maqueda et al.[43,44] determines both the kinetic model and the parameter set of the Arrhenius equation (3). This method is based on the logarithmic form of the general kinetic equation:

$$\ln \frac{(d\alpha/dt)}{f(\alpha)} = \ln A - \frac{E}{R}\frac{1}{T} \tag{6}$$

The combined kinetic method can be used to test several kinetic models simultaneously. First, the kinetic model and its parameters are selected. Then the left-hand side of Equation (6) is calculated for a particular kinetic model and plotted as a function of reciprocal temperature. The correct model and parameters should give a linear dependence. Arrhenius parameters A and E are obtained by linear regression (that is, the intercept and slope, respectively). On the contrary, the incorrect model or parameters produce a distorted nonlinear dependence.

As already mentioned, the JMAK theory is the most widely used model to describe crystallization in glasses:[5–9,40]

$$f(\alpha) = m \cdot (1-\alpha) \cdot [-\ln(1-\alpha)]^{1-(1/m)} \tag{7}$$

The parameter m in Equation (7) depends on the nucleation mechanism and crystal growth. It is quite successful under isothermal conditions, where randomly dispersed nuclei crystallize in the volume of the sample. Nevertheless, when the initiation of the growth process involves the development of a large number of closely spaced nuclei on all surfaces, the kinetic characteristics of the overall kinetic process are determined by the geometry of the crystallization interface that advances from these boundaries to the center of the particle.[12,45] This is often referred to as the "contracting sphere" model (R3) and is described by[45]

$$f(\alpha) = (1-\alpha)^{2/3} \tag{8}$$

2.3 | Description of crystal growth

For many chalcogenide systems, the crystal growth rate u measured by microscopy can be described in a narrow temperature range using an Arrhenius-type equation:[30–32]

$$u(T) = A_G \cdot e^{-\frac{E_G}{RT}} \tag{9}$$

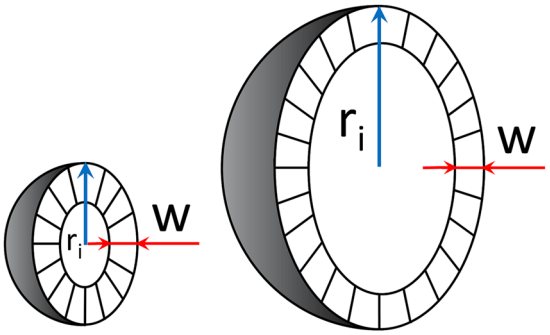

FIGURE 1 Illustration of surface crystallization of a spherical grain of glass of different radius r_i (R3 model); the thickness w of the crystalline layer is emphasized.

where A_G is the preexponential factor and E_G is the activation energy of the crystal growth.

Assuming a spherical grain of glass with radius r, the volume of the grain V is given by $V = (4/3)\pi r^3$. Crystallization begins with surface nuclei and creates a crystalline layer of thickness w as shown in Figure 1. Thus, the volume of the noncrystalline phase is $V_n = (4/3)\pi(r-w)^3$, so the conversion takes the form

$$\alpha = \frac{V_{cr}}{V} = 1 - \frac{V_n}{V} = 1 - \left(\frac{r-w}{r}\right)^3 \tag{10}$$

where V_{cr} is the volume of the crystalline phase. Differentiating Equation (10) with respect to time and assuming $w = u \cdot t$, the crystallization rate can be expressed as:

$$\frac{d\alpha}{dt} = \frac{3u}{r}\left(\frac{r-w}{r}\right)^2 = \frac{3u}{r}(1-\alpha)^{2/3} \tag{11}$$

Substituting $f(\alpha)$ for the R3 model (Equation 8 into Equation 2) and comparing the result with Equation (11) gives

$$u(T) = \frac{r}{3} \cdot k(T) \tag{12}$$

Similarly, we can express the preexponential factor in Equation (9) as $A_G = (r/3) \cdot A$. Therefore, the kinetic parameters of the R3 model obtained from the DSC curve can be directly compared with the measured crystal growth rate. However, the recalculation requires that the exact particle size be known.

2.4 | Simulation of DSC curves

The DSC calorimetric curve can be simulated when the temperature dependence of the crystal growth rate (i.e., Equation 9) is given. Then, the thickness of the surface crystalline layer can be calculated for a given time and temperature by:

$$w = \int u(T) \cdot dt \tag{13}$$

Subsequently, assuming a particle radius r, the heat flow is determined by combining Equations (1) and (11), and using the experimentally determined enthalpy change of crystallization ($\Delta H = 47.1 \pm 0.4$ J g^{-1}).

For particles of nonuniform size, as shown in Figure 1, the conversion is strongly dependent on particle size. The particles are separated into fractions with radius r_i based on the experimental particle size distribution. Each fraction contains N_i particles of the volume V_i. The volume ratio x_i of the fraction in the sample is calculated by

$$x_i = \frac{N_i \cdot V_i}{\sum N_i \cdot V_i} \tag{14}$$

Using Equation (11), the simulated DSC curve for the overall powder is given by

$$\Phi = \Delta H \cdot \sum x_i \frac{d\alpha_i}{dt} \tag{15}$$

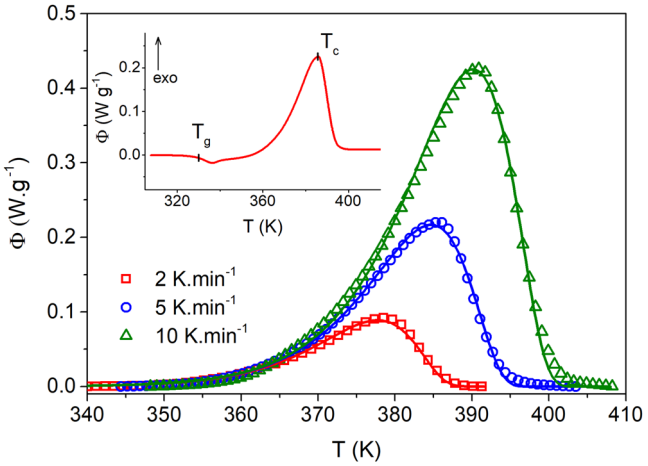

FIGURE 2 Heat flow as a function of temperature for experimental data (points) and fits (solid lines) using the R3 model, optimized for the distribution of the particles in the powder sample as described in Section 4. The inset shows the complete differential scanning calorimetry (DSC) curve for a heating rate of 5 K min^{-1}.

3 | RESULTS

The crystallization kinetics of a model chalcogenide glass were measured by using the nonisothermal DSC method. Measurements were made in fine powder with 20–50 μm grain size. Figure 2 shows typical DSC crystallization curves taken at various heating rates (points). The inset of Figure 2 shows that the crystallization process begins immediately above the glass transition region (T_g = 330

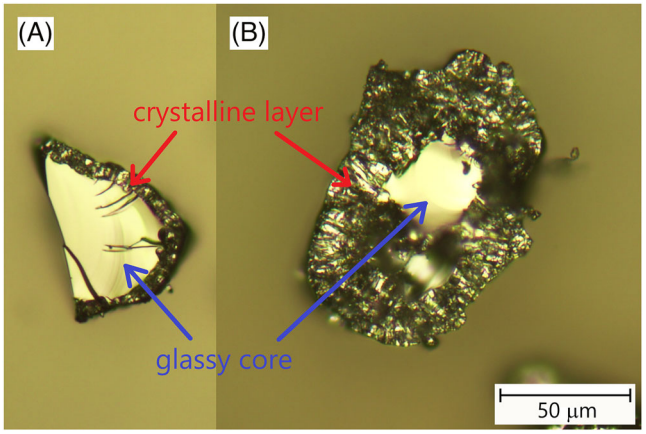

FIGURE 3 Microphotographs of cross-section of a powder grains held at 368 K for 20 min (A) and 60 min (B). The scale is identical.

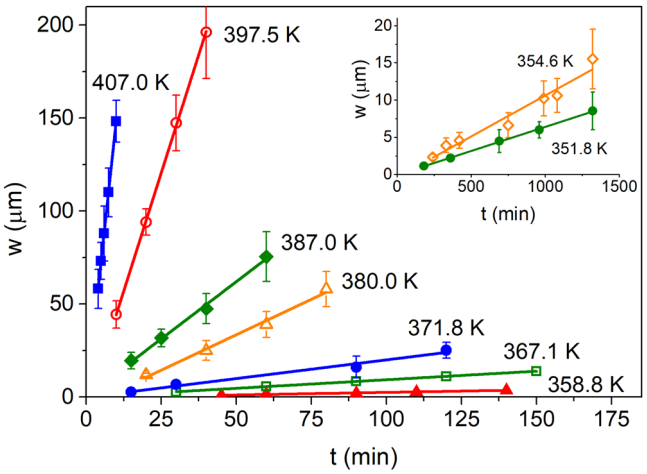

FIGURE 4 Thickness of crystalline layer on the surface as a function of time and at different temperatures. The inset shows experimental data for lower temperatures.

K). As expected, the maximum of the crystallization peak shifts as the heating rate increases. However, the starting point of the crystallization peaks remains relatively constant. This behavior differs from that observed for other compositions of $Se_{100-x}Te_x$ glasses ($x = 5$, 10, and 20)[46,47] and indicates a different mechanism of crystallization.

To analyze the kinetic results obtained by DSC in more detail, we performed an independent study of crystal growth by microscopy. Several fine powders were prepared and subsequently annealed at 368 K for different periods of time. A fresh fracture of two grains annealed at this temperature for 20 and 60 minutes is shown in Figure 3A,B, respectively. The crystalline layer and glassy core are clearly seen. The thickness of the crystalline layer in Figure 3B is three times higher than that in Figure 3A, corresponding to a longer annealing time. The core of both grains remains glassy, as proved by the reflectance. Therefore, it seems that crystal growth in fine powder takes place mainly in the surface layer and that the glassy core of the grain does not contain any measurable crystal inclusions.

To determine the rate of growth of the surface layer as a function of temperature, crystal growth was measured by optical microscopy in the temperature range 352−407 K, which corresponds to the temperature range of DSC crystallization peaks. For accurate sample handling, bulk samples were used, which were annealed for a period of time, then broken, and the thickness of the surface crystalline layer w was determined (as depicted in Figure 1). The thickness w of the crystalline layer grew linearly in time for all temperatures tested, as illustrated in Figure 4. Their intercepts are all close to zero, which indicates growth from pre-existing nuclei. Barták et al.[39] reported similar behavior for crystals growing in the volume of a $Se_{70}Te_{30}$ sample.

TABLE 1 Growth rates of the surface crystalline layer at different temperatures determined from the data shown in Figure 4.

T (K)	u (µm min^{-1})
351.8	0.00647 ± 0.00013
354.6	0.0110 ± 0.0010
358.8	0.0274 ± 0.0014
367.1	0.0921 ± 0.0006
371.8	0.201 ± 0.019
380.0	0.762 ± 0.050
387.0	1.231 ± 0.054
397.5	5.087 ± 0.059
407.0	14.986 ± 0.073

The crystal growth rate of the surface layer corresponds to the slope of the layer thickness in terms of time. The crystal growth rates for surface crystallization in $Se_{70}Te_{30}$ glass are summarized in Table 1.

4 | DISCUSSION

4.1 | Standard kinetic analysis of nonisothermal DSC data

The nonisothermal DSC data shown in Figure 2 were analyzed using several methods to determine the most reliable kinetic model. The combined kinetic method[43,44] provides linear fits of the plot of $\ln[(d\alpha/dt)/f(\alpha)]$ versus reciprocal temperature for both the JMAK and R3 models (with confidence bands of 99%), as shown in Figure 5. The Arrhenius parameters can be calculated from Equation (6) for the JMAK model ($E = 150.2 \pm 1.6$ kJ mol^{-1}, $\ln A = 42.4 \pm 0.5$,

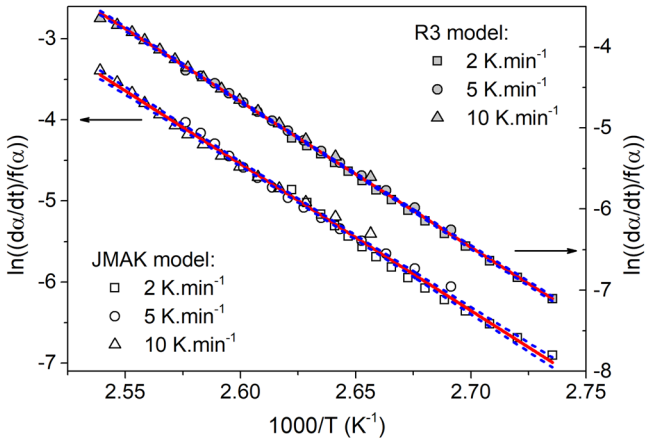

FIGURE 5 Results of combined kinetic analysis for the R3 and Johnson–Mehl–Avrami–Kolmogorov (JMAK) models (solid line; dashed lines correspond to confidence bands 99%; the points are to experimental data).

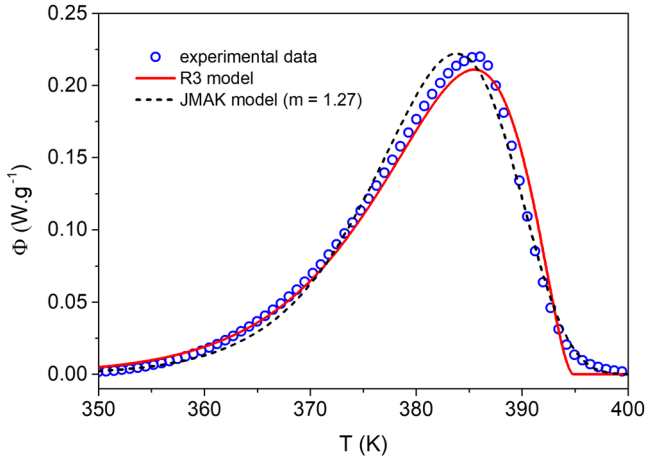

FIGURE 6 Nonisothermal differential scanning calorimetry (DSC) curves of crystallization in $Se_{70}Te_{30}$ glass (20–50 μm powder, 5 K min^{-1}). The experimental data are plotted as points, and the lines represent the theoretical curves of the R3 model (solid line) and the Johnson–Mehl–Avrami–Kolmogorov (JMAK) model (dashed line).

m = 1.27) and the R3 model (E = 149.3 ± 0.8 kJ mol^{-1}, ln A = 42.0 ± 0.3). Although this method gives a slightly better fit for the R3 model than for the JMAK model (see Figure 5), it is difficult to distinguish between them. Figure 6 shows a comparison of the calculated DSC curves (lines) for both the R3 and the JMAK models with experimental data (points). Both models differ slightly from the measured data. Although the JMAK model overestimates a leading part of the DSC curve and its maximum is shifted to lower temperatures, the R3 model does not fit well the decreasing part of the DSC curve, especially the peak tail. Additional analysis is needed to decide which model describes the best experimental data. Two methods

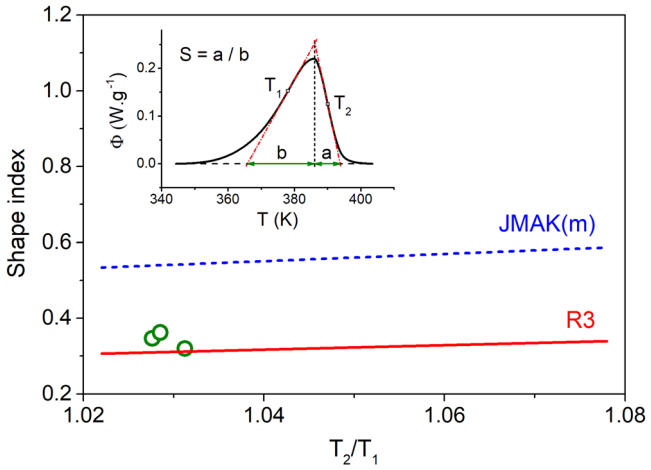

FIGURE 7 The shape index as a function of the characteristic inflection temperature ratio T_2/T_1 for experimental data (green points) and theoretical lines corresponding to the Johnson–Mehl–Avrami–Kolmogorov (JMAK) (blue dashed line) and R3 (red solid line) models. The inset shows the determination of the shape index from experimental curve (β = 5 K min^{-1}).

of kinetic analysis, the shape index analysis[41,48] and the $y(\alpha)$ and $z(\alpha)$ master plots,[40,42] were used for their high sensitivity to the symmetry of DSC curves.

The determination of the shape index S[41,48] from the experimental data is illustrated in the inset of Figure 7. The dependence of the shape index S on the inflection temperature ratio (T_2/T_1) of the DSC curve is a characteristic fingerprint for the kinetic model.[48] Figure 7 shows theoretical prediction (lines) for the JMAK (blue dashed line) and R3 (red solid line) models. The transformed experimental data are then shown for all heating rates (green points). The experimental data points are significantly closer to the symmetry expected for the R3 model than for the JMAK model. Therefore, it seems that the R3 model is more suitable for the description of this crystallization process.

Another convenient method to determine the most suitable kinetic model is based on normalized functions $y(\alpha)$ and $z(\alpha)$.[40,42] Figure 8 shows these functions obtained by conversion of experimental DSC data using Equations (4) and (5) for E = 150 kJ mol^{-1}. The experimental data points are much closer to the prediction of the R3 model (see the solid line in Figure 8A), showing the maximum at $a_z^* \approx 0.716$, whereas the expected value for the JMAK model (dashed line in Figure 8A) is $a_z^* \approx 0.632$.[40] The normalized function $y(\alpha)$ is more sensitive to the symmetry of the DSC curve. The theoretical curves of models R3 (solid line), JMAK (m = 1) (dotted line) and JMAK (m = 1.27) (dashed line) are plotted in Figure 8B. The difference between models is evident. Kinetic models based on the JMAK equation influence the shape of the DSC

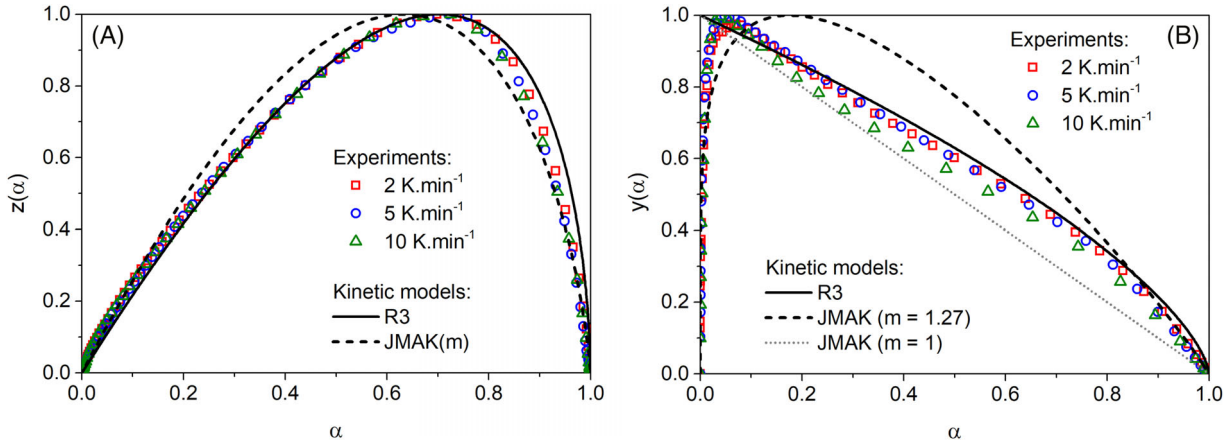

FIGURE 8 The $z(\alpha)$ (A) and the $y(\alpha)$ (B) as a function of conversion. The points correspond to the experimental data. The solid line corresponds to the R3 model, and the dashed and dotted lines correspond to the models Johnson–Mehl–Avrami–Kolmogorov (JMAK) ($m = 1.27$) and JMAK ($m = 1$), respectively.

curves depending on the parameter m. The JMAK model for $m = 1$ exhibits a linear function $y(\alpha)$ that is close to the R3 model for low values of α. For this reason, the JMAK model has been used for the description of a surface crystallization process, even though it was originally derived for the crystal growth at volume nuclei.[49] Figure 8B reveals that the experimental data clearly correspond to the R3 model. The same result provides a comparison of the calculated and experimental $z(\alpha)$ functions, as shown in Figure 8A. Therefore, the inspection of the $y(\alpha)$ and $z(\alpha)$ dependences leads to the same conclusion as that obtained from the shape index analysis, that is, the dominant surface crystallization process in a fine powder of $Se_{70}Te_{30}$ glass.

Svoboda and Málek[50] described a similar behavior of the function $y(\alpha)$ for the same powder fraction of $Se_{70}Te_{30}$ but not for other Se–Te compositions.[46,47] However, in the present study, a characteristic profile of the R3 model is more evident. Therefore, the JMAK nucleation growth model is not appropriate for describing the experimental data, whereas the R3 model, which corresponds to the surface crystallization process, reproduces the data significantly better.

4.2 | Comparison of nonisothermal and isothermal DSC data

To validate our conclusions from nonisothermal DSC data, we analyzed previously reported isothermal crystallization data for the same powder fraction of $Se_{70}Te_{30}$.[51] Figure 9 shows previously reported experimental data for an isothermal measurement at 363 K (points) and the curves simulated for the R3 model. The crystallization rate constant $k = 0.0503\ \text{min}^{-1}$ was obtained by optimization

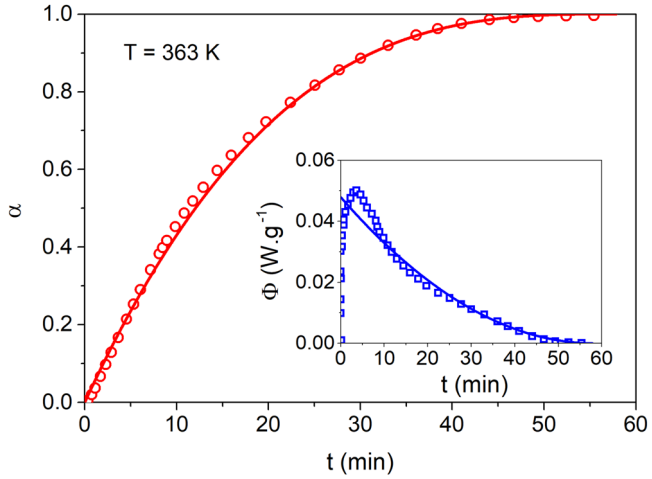

FIGURE 9 Degree of crystallization as a function of time extracted from isothermal differential scanning calorimetry (DSC) data at 363 K from Ref.[51] (points) and theoretical curve (line) of the R3 model. The inset shows the original heat flow data (points) and the theoretical curve (line).

and enthalpy $\Delta H = 55.9\ \text{J g}^{-1}$ was determined by integration of the DSC peak. As observed in this figure, both curves match except for an initial part of the DSC curve. The degree of crystallization as a function of time does not exhibit a noticeable inflection point, as is typical for the R3 model. Therefore, the R3 model describes the kinetics of crystallization of $Se_{70}Te_{30}$ glass with 20–50 μm particle size both under nonisothermal and isothermal conditions.

4.3 | Effect of particle size distribution

Kinetic analysis of the crystallization curves of the DSC of fine powder $Se_{70}Te_{30}$ glass indicates that the most

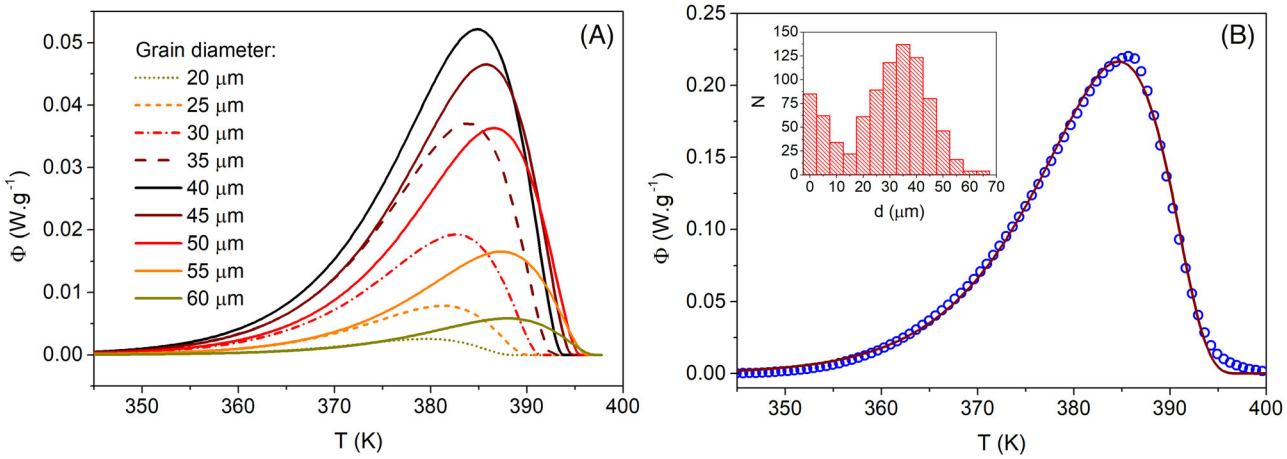

FIGURE 10 (A) Simulated differential scanning calorimetry (DSC) curves for various particle sizes, including their volume ratio in powder (heating at 5 K min^{-1}). (B) Simulated DSC curve for the overall powder fraction 20–50 μm (line) and experimental points. The inset plot shows the experimental histogram of the particle size distribution.

probable kinetic model R3 can be used for a description of the surface crystallization process. This conclusion was verified by microscopy as shown in Figure 3. However, we still need to explain the slight deviation of the non-isothermal DSC data from the theoretical curve at the tail of the DSC peak, as mentioned earlier (see Figure 6). Contrary to the JMAK kinetic model, the R3 model is significantly affected by grain size, as illustrated in Figure 1. Therefore, the deviation from the theoretical prediction for the R3 model from the experimental data could likely be attributed to the nonuniformity of the particle size distribution in the $Se_{70}Te_{30}$ glass powder sample. The ideal kinetic model assumes a single size and ideal shape of the particle, which is hardly achievable in a real system. Koga and Criado[52,53] studied the role of the grain size distribution in various kinetic models and reported that although the grain size distribution strongly affects the preexponential factor and the shape of the kinetic curve, it does not significantly affect the activation energy. The particle size distribution has also been shown to be important in correctly describing the dehydroxylation of kaolinite,[54] and the thermal behavior of muscovite and biotite.[55] The next section examines how the particle size distribution affects the crystallization of the $Se_{70}Te_{30}$ glass powder.

As mentioned above, the effect of the particle size distribution on DSC crystallization curves should be considered for a proper kinetic analysis. Figure 10A shows a set of curves simulated using the method described in Section 2.4, the optimized kinetic parameters $E_G = 152.7$ kJ mol^{-1}, $\ln A_G = 31.2$ and the particle sizes corresponding to the experimental particle size distribution determined by optical microscopy (inset in Figure 10B). The area of the DSC curves corresponds to the volume ratio of the real powder fraction. The size plays a significant role in the overall temperature of the process. Actually, the maxima of these curves shift to higher temperatures with increasing particle diameter. Figure 10B shows the simulated DSC curve, which is a weighted sum of the contribution of all particle size fractions (line). The points correspond to the experimental data. If the particle size distribution is considered in the calculation, the overall curve matches the experimental data very well in the entire temperature range (Figure 10B). Although the smallest particles (<20 μm) in the powder are quite numerous (see the histogram in Figure 10B), they correspond to a small part (<0.3%) of the total volume of the sample alone and therefore do not significantly affect the resulting DSC curve. In contrast, larger particles considerably affect the tail of the DSC peak. Identical results were obtained for all DSC curves obtained for different heating rates and are depicted in Figure 2. In all cases, the agreement between experimental and simulated curves (solid lines) is very good when the particle size distribution is considered for optimization of kinetic parameters.

4.4 | Comparison of DSC data with microscopic crystal growth

It is interesting to compare quantitatively indirect DSC experiments that provide the heat flow associated with the crystallization under linear heating conditions with direct isothermal measurement of crystal growth determined by microscopy. Previous studies in the literature on the crystallization of $BiFeO_3$ by combined DSC and high-temperature XRD analysis have shown that a proper kinetic analysis allows extracting equivalent kinetic parameters from different experimental methods.[56]

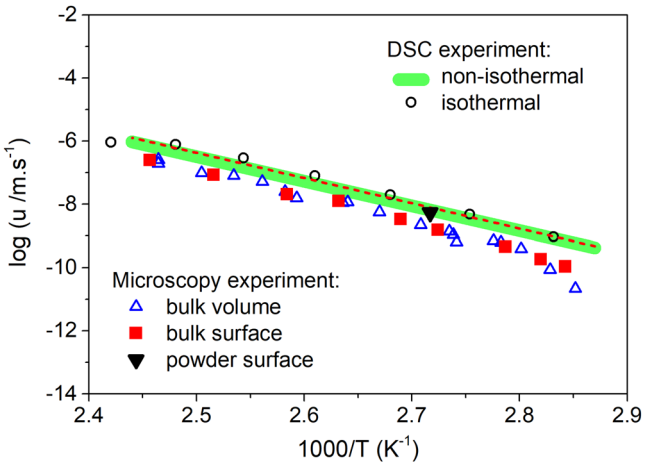

FIGURE 11 The logarithm of the crystal growth rate u measured by microscopy as a function of the reciprocal temperature for the surface crystalline layer in bulk (red squares) and powder sample (black triangle) reported here and for the crystals in volume of glass (blue triangles) reported in Ref.[39]. The thick green line corresponds to the crystal growth rate calculated from the differential scanning calorimetry (DSC) results applying Equation (12) for a grain size of 20–50 μm. The dashed line represents the parameters of the nonisothermal DSC curve optimized for a given histogram of the powder size distribution. The open circles correspond to data calculated from the isothermal DSC experiments reported in Ref.[51] The size of the data points is comparable to the estimated experimental error.

Figure 11 compares the surface crystal growth rate in bulk glass $Se_{70}Te_{30}$ measured by optical microscopy and listed in Table 1 (red squares) with that extracted from the DSC data. Our surface crystal growth measurement is consistent with data previously reported by Barták et al.[39] for the crystal growth rate measured inside the bulk sample (see blue triangles in Figure 11). The parameters of the R3 model obtained by combined kinetic analysis of nonisothermal DSC data are transformed by Equation (12), assuming the average diameter of powder particle $d = 35$ μm, and plotted by a thick green line in Figure 11. The width of this line corresponds to the particle size ranging from 20 to 50 μm. The dashed line shows the optimized crystal growth rate as a function of temperature for the particle size distribution model ($E_G = 152.7 \pm 0.8$ kJ mol^{-1}, ln $A_G = 31.2 \pm 0.3$). This line is very close to previously reported isothermal DSC data[51] interpreted within the R3 model in this work and transformed by Equation (12) for an average particle size of 35 μm (open circles). Although the activation energy of crystallization obtained from microscopy and DSC analysis is nearly the same (at least within the combined margin of experimental error), the logarithmic preexponential factor of the crystal growth rate differs significantly (by a factor $r/3$) compared to the combined kinetic analysis for the R3 model. This result resembles the previously reported finding by Koga and Criado.[52,53]

It follows that the crystal growth rate in glassy $Se_{70}Te_{30}$ (bulk) is the same for surface and volume crystals. The values of u determined from DSC data shift only slightly to higher crystal growth rates, which is probably explained by the fact that additional surface nuclei are created by mechanical crushing of bulk glass into finer powder, which eventually leads to slightly higher crystal growth rates. This slight increase in the crystallization rate was verified by measuring the thickness of the crystalline layer in the powder particle (black triangle in Figure 11). The R3 model assumes ideal spherical particles. However, in a real sample, a larger fractal surface might be expected. This could be another source of discrepancy between the model and the real data. However, the values calculated from the isothermal and nonisothermal DSC data for the R3 model are consistent with the crystal growth rates directly observed in bulk and powder of $Se_{70}Te_{30}$.

5 | CONCLUSIONS

The crystallization kinetics in chalcogenide glass in fine powder (20–50 μm) of $Se_{70}Te_{30}$ composition was studied using DSC and optical and infrared microscopy. A complex kinetic analysis of these experimental data was performed with an emphasis on methods of kinetic analysis more sensitive to the shape of the DSC curve. The analysis reveals that the contracting sphere mechanism (R3 model) is the rate determining step of surface crystal growth in this crystallization process. The preexponential factor for this model strongly depends on the grain size of the sample. Therefore, the particle size distribution has been taken into account. The crystallization kinetics for a fine powder of $Se_{70}Te_{30}$ glass determined from nonisothermal DSC data are consistent with previously reported isothermal crystallization data for the same powder fraction. The crystal growth rate calculated from isothermal and nonisothermal DSC data is consistent with the microscopically measured surface and bulk crystal growth rates. The complex analysis procedure described in this paper allows to determine the crystallization mechanism and crystal growth rates from DSC data without the need to directly monitor crystal growth in such chalcogenide glasses (and sample forms) where surface crystallization is dominant.

ACKNOWLEDGMENTS

This work was supported by the Selected Research Teams Program of the Faculty of Chemical Technology, University of Pardubice. The authors thank Petr Pilný for providing the OriTas software, which was used for some of the

kinetic calculations. The research grant PDC2021-121552-C21 (MCIN/AEI/10.13039/501100011033 and the European Union Next Generation grant EU/PRTR) is acknowledged.

ORCID

Jana Shánělová https://orcid.org/0000-0001-5517-7434
Pavla Honcová https://orcid.org/0000-0003-1330-3206
Jiří Málek https://orcid.org/0000-0002-7502-5320
Antonio Perejón https://orcid.org/0000-0002-5525-2227
Luis A. Pérez-Maqueda https://orcid.org/0000-0002-8267-3457

REFERENCES

1. Zanotto ED. Glass crystallization research—a 36-year retrospective. Part I, fundamental studies. Int J Appl Glass Sci. 2013;4:105–16.
2. Shekunov B. Kinetics of crystallization and glass transition in amorphous materials. Cryst Growth Des. 2020;20:95–106.
3. Glicksman ME. Principles of solidification. An introduction to modern casting and crystal growth concepts. New York: Springer; 2011.
4. Singh AK. Crystallization kinetics of chalcogenide glasses. In: Andreeta M, editor. Chapter 2 in Crystallization—science and technology. Rijeka, Croatia:InTech; 2012. p. 29–64. https://doi.org/10.5772/34989
5. Johnson WA, Mehl KF. Reaction kinetics in processes of nucleation and growth. Trans Am Inst Min Metall Eng. 1932;135:416–62.
6. Kolmogorov AN. On the statistical theory of metal crystallization. Izv Akad Nauk SSSR Ser Mat. 1937;3:355–60.
7. Avrami M. Kinetics of phase change: I. General theory. J Chem Phys. 1939;7:1103–12.
8. Avrami M. Kinetics of phase change: II. Transformation-time relations for random distribution of nuclei. J Chem Phys. 1940;8:212–24.
9. Avrami M. Kinetics of phase change: III. Granulation, phase change, and microstructure. J Chem Phys. 1941;9:177–84.
10. Málek J, Mitsuhashi T. Testing method for the Johnson–Mehl–Avrami equation in kinetic analysis of crystallization processes. J Am Ceram Soc. 2000;83:2103–5.
11. Villa E, Rios PR. Transformation kinetics for surface and bulk nucleation. Acta Mater. 2010;58:2752–68.
12. Müller R. The influence of grain size on the overall kinetics of surface-induced glass crystallization. J Therm Anal. 1989;35:823–35.
13. Weinberg MC. Transformation kinetics of particles with surface and bulk nucleation. J Non-Cryst Solids. 1992;142:126–32.
14. Reis RMCV, Zanotto ED. Simple model for particle phase transformation kinetics. Acta Mater. 2018;154:228–36.
15. Ferreira EB, Lopez-Richard V, Zanotto ED, Marques GE. Analytical model for heterogeneous crystallization kinetics of spherical glass particles. J Am Ceram Soc. 2009;92:2616–8.
16. Marques LE, Costa AMC, Crovace MC, Rodrigues ACM, Cabral AA. Influence of particle size on nonisothermal crystallization in a lithium disilicate glass. J Am Ceram Soc. 2015;98:774–80.
17. Alencar MVS, Bezerra GVP, Silva LD, Schneider JF, Pascual MJ, Cabral AA. Structure, glass stability and crystallization activation energy of SrO–CaO–B_2O_3–SiO_2 glasses doped with TiO_2. J Non-Cryst Solids. 2021;554:120605.
18. Bezerra GVP, Alencar MVS, Crovace MC, Rodrigues AM, Cabral AA. Anomalous Avrami index recorded during the non-isothermal crystallization of borotitanosilicate glass powders. J Non-Cryst Solids. 2023;600:122008.
19. Svoboda R. Kinetic analysis of particle-size based complex kinetic processes. J Non-Cryst Solids. 2020;533:119903.
20. Fernandes RG, Ferreira EB. The shape of diopside glass particles probed by the non-isothermal crystallization kinetics and differential scanning calorimetry. J Non-Cryst Solids. 2018;497:63–70.
21. Fernandes RG, Reis RMCV, Tobar RR, Zanotto ED. Acta Mater. 2019;175:130–9.
22. Ray CS, Fang X, Day DE. New method for determining the nucleation and crystal-growth rates in glasses. J Am Ceram Soc. 2000;83:865–72.
23. Ray CS, Ranasinghe KS, Day DE. Determining crystal growth rate-type of curves in glasses by differential thermal analysis. Solid State Sci. 2001;3:727–32.
24. Reis RMCV, Fokin VM, Zanotto ED. Determination of crystal growth rates in glasses over a temperature range using a single DSC run. J Am Ceram Soc. 2016;99:2001–8.
25. Reis RMCV, Ghussn L. Single-run DSC method for determining surface crystal growth rate in glasses generalized for samples of different shapes. J Am Ceram Soc. 2020;104:2077–86.
26. Henderson DW, Ast DG. Viscosity and crystallization kinetics of As_2Se_3. J Non-Cryst Solids. 1984;64:43–70.
27. Málek J, Černošková E, Švejka R, Šesták J, Van der Plaats G. Crystallization kinetics of $Ge_{0.3}Sb_{1.4}S_{2.7}$ glass. Thermochim Acta. 1996;280–281:353–61.
28. Zhang W, Mazzarello R, Wuttig M, Ma E. Designing crystallization in phase-change materials for universal memory and neuro-inspired computing. Nat Rev Mater. 2019;4:150–68.
29. Orava J, Greer AL, Gholipour B, Hewak DW, Smith CE. Characterization of supercooled liquid $Ge_2Sb_2Te_5$ and its crystallization by ultrafast-heating calorimetry. Nat Mater. 2012;11:279–83.
30. Málek J, Barták J, Shánělová J. Spherulitic crystal growth velocity in selenium supercooled liquid. Cryst Growth Des. 2016;16:5811–21.
31. Málek J, Shánělová J, Martinková S, Pilný P, Koštál P. Crystal growth velocity in As_2Se_3 supercooled liquid. Cryst Growth Des. 2017;17:4990–9.
32. Málek J, Podzemná V, Shánělová J. Crystal growth kinetics in GeS_2 glass and viscosity of supercooled liquid. J Phys Chem B. 2021;125:7515–26.
33. Honcová P, Valdés D, Barták J, Málek J, Pilný P, Slang S. Combination of indirect and direct approaches to the description of complex crystallization behavior in $GeSe_2$-rich region of pseudobinary $GeSe_2$–Sb_2Se_3 system. J Non-Cryst Solids. 2021;568:120968.
34. Svoboda R, Prikryl J, Cicmancova V, Prokop V, Kolobov AV, Krbal M. Crystal growth in amorphous selenium thin films—reviewed and revisited: direct comparison of microscopic and calorimetric measurements. Cryst Growth Des. 2021;21:7087–97.
35. Svoboda R, Prikryl J, Provotorov P, Kolobov AV, Krbal M. Crystal growth in Se–Te chalcogenides: overview of the growth/relaxation/viscosity interplay for bulk glasses and thin films. Cryst Growth Des. 2023;23:216–28.

36. Honcová P, Shánělová J, Barták J, Málek J, Koštál P, Stehlík S. General approach to the nucleation and crystal growth in $Sb_{0.5}Se_{99.5}$ glass explaining the shape of DSC curves. Cryst Growth Des. 2016;16:2904–11.
37. Svoboda R, Honcová P, Málek J. Enthalpic structural relaxation in Te–Se glassy system. J Non-Cryst Solids. 2011;357:2163–9.
38. Pilný P. OriTas 2016—all-in-one solution for kinetic analysis of thermoanalytical data. 2016. Available from: http://www.petrpilny.cz/oritas-eng/
39. Barták J, Martinková S, Málek J. Crystal growth kinetics in Se–Te bulk glasses. Cryst Growth Des. 2015;15:4287–95.
40. Málek J. Kinetic analysis of crystallization processes in amorphous materials. Thermochim Acta. 2000;355:239–53.
41. Málek J. The shape of thermoanalytical curves as a function of the reaction kinetics. Thermochim Acta. 1993;222:105–13.
42. Málek J, Mitsuhashi T, Criado JM. Kinetic analysis of solid-state processes. J Mater Res. 2001;16:1862–71.
43. Pérez-Maqueda LA, Criado JM, Málek J. Combined kinetic analysis for crystallization kinetics of non-crystalline solids. J Non-Cryst Solids. 2003;320:84–91.
44. Pérez-Maqueda LA, Criado JM, Sánchez-Jiménez PE. Combined kinetic analysis of solid-state reactions: a powerful tool for the simultaneous determination of kinetic parameters and the kinetic model without previous assumptions on the reaction mechanism. J Phys Chem A. 2006;110:12456–62.
45. Bamford CH, Tipper CFH. Comprehensive chemical kinetics. Reaction in the solid state. Vol 22. Elsevier. ISBN 0-0444-41807-5.
46. Svoboda R, Krbal M, Málek J. Crystallization kinetics in Se–Te glassy system. J Non-Cryst Solids. 2011;357:3123–9.
47. Svoboda R, Málek J. Crystallization mechanisms occurring in the Se–Te glassy system. J Therm Anal Calorim. 2015;119:155–66.
48. Málek J, Criado JM. The shape of a thermoanalytical curve and its kinetic information content. Thermochim Acta. 1990;164:199–209.
49. Svoboda R. Usage of masterplots in kinetic analysis of complex surface/volume crystallization processes in Se–Te glasses. J Non-Cryst Solids. 2020;541:120068.
50. Svoboda R, Málek J. Interpretation of crystallization kinetics results provided by DSC. Thermochim Acta. 2011;526:237–51.
51. Svoboda R, Málek J. Particle size dependent isothermal crystallization kinetics in a Se–Te glassy system. Thermochim Acta. 2015;610:47–56.
52. Koga N, Criado JM. Influence of the particle size distribution on the CRTA curves for the solid state reactions of interface shrinkage type. J Therm Anal. 1997;49:1477–84.
53. Koga N, Criado JM. Kinetic analyses of solid-state reactions with particle-size distribution. J Am Ceram Soc. 1998;81:2901–9.
54. Arcenegui-Troya J, Sánchez-Jiménez PE, Perejón A, Pérez-Maqueda LA. Relevance of particle size distribution to kinetic analysis: the case of thermal dehydroxylation of kaolinite. Processes. 2021;9:1852.
55. Pérez-Maqueda LA, Blanes JM, Pascual J, Pérez-Rodríguez JL. The influence of sonification on the thermal behavior of muscovite and biotite. J Eur Ceram Soc. 2004;24:2793–801.
56. Gil-González E, Perejón A, Sánchez-Jiménez PE, et al. Crystallization kinetics of nanocrystalline materials by combined X-ray diffraction and differential scanning calorimetry experiments. Cryst Growth Des. 2018;18:3107–16.

How to cite this article: Shánělová J, Honcová P, Málek J, Perejón A, Pérez-Maqueda LA. Direct comparison of surface crystal growth kinetics in chalcogenide glass measured by microscopy and DSC. J Am Ceram Soc. 2023;106:6051–6061. https://doi.org/10.1111/jace.19204